JOURNAL OF CATALYSIS 93, 122–134 (1985)

Catalytic Hydrodemetallation of Nickel Porphyrins

II. Effects of Pyridine and of Sulfiding

ROBERT A. WARE[1] AND JAMES WEI[2]

Department of Chemical Engineering, Massachusetts Institute of Technology, Cambridge, Massachusetts 02139

Received March 29, 1984; revised November 27, 1984

The hydrodemetallation (HDM) reaction of a model nickel compound, Ni-tetra(3-methylphenyl)porphyrin (Ni-T3MPP), has been investigated with pyridine over the oxide form of $CoMo/Al_2O_3$ catalyst and without pyridine over the sulfided catalyst. The HDM pathway for Ni-T3MPP was unchanged from that previously reported on the clean (N + S free) oxide catalyst: initial ring hydrogenation followed by the final ring cleavage and metal deposition. Marked differences were observed in the hydrogenation/ring cleavage selectivity, suggesting a dual-site catalyst. Pyridine strongly inhibited the hydrogenation sites and showed less inhibition on hydrogenolysis. Sulfiding strongly enhanced the ring cleavage steps and showed less enhancement on hydrogenation. The high bond-cleavage activity was interpreted in terms of Brønsted acidity arising from the dissociation of H_2S on Mo vacancies. Metal-deposition profiles measured under diffusion-limited conditions on the sulfided catalyst were modeled using diffusivities on the order of 10^{-6} cm²/sec. The enhanced metal-deposition activity of the sulfided catalyst compared to the oxide catalyst was manifested in steeper, more U-shape profiles with less deposit in the center of the pellets.

1. INTRODUCTION

The metals nickel and vanadium in crude oil are the most troublesome of the heteroatoms in quantities ranging from just 10 to over 1000 ppm by weight of Ni and V (*1*). In current refining technology these metals are often removed during a hydrodesulfurization (HDS) or hydrodenitrogenation (HDN) process by reaction at high temperature and hydrogen pressure, leading to deposition of the metal on alumina-supported CoMo or NiMo catalyst.

In Part I (*2*) of this series, the hydrodemetallation (HDM) reaction behavior of a series of nickel porphyrins characteristic of the metal-bearing species in residuum oil was investigated on an oxide $CoMo/Al_2O_3$ catalyst in a clean (N + S free) environment. This provided an understanding of the porphyrin demetallation reactions in the absence of external artifacts or competing reactions. The metallo-porphyrins were determined to undergo structural changes involving, initially, loss of aromatic character by hydrogenation prior to cleavage of the ring and deposition of the metal. The substitution pattern on the periphery of the metallo-porphyrins was shown to significantly influence the complexity of the reaction pathway and the relative rates of hydrogenation and metal deposition.

Industrial demetallation processing occurs in the presence of nitrogen and sulfur compounds on sulfided catalysts, so it is desirable to investigate model compound HDM behavior under more industrially realistic conditions. It is important to verify that structure/reactivity patterns elucidated in the clean model compound environment are applicable in more complex environments.

The information published in the literature on the demetallation of metallo-porphyrins on sulfided catalysts has been lim-

[1] Present address: Mobil Research and Development Corp., Paulsboro, N.J. 08066.

[2] To whom correspondence should be addressed.

0021-9517/85 $3.00

ited. The examination of these reactions in the presence of heterocyclic nitrogen compounds common to petroleum oil (typically pyridine or quinoline) has not previously been reported.

Complementing the model compound demetallation work presented in Part I (*2*), Rankel (*3, 4*) has investigated the reaction pathway of nickel etioporphyrin and nickel and vanadyl tetraphenylporphyrin in the presence of H_2 and H_2S, both under thermal and catalytic (sulfided CoMo catalyst) conditions. In the absence of a catalyst, reaction with H_2S was reported to produce cleaved porphyrin rings, or polypyrrolics, identified on the basis of uv–visible spectra. Vanadyl porphyrins were more reactive than their nickel analogs. Reactions catalyzed by sulfided CoMo in the presence of H_2 and H_2S produced hydrogenated metallo-porphyrins and polypyrrolics. Metal-free porphyrin structures were not observed as intermediates in the catalytic reactions in agreement with the earlier results of Hung and Wei (*5*) on the oxide catalyst. The catalytic hydrogenative route was determined by Rankel to be the dominant pathway for metallo-porphyrin demetallation.

Model compound work by Kameyama *et al.* (*6, 7*) in the presence of sulfur confirmed the sequential mechanism for HDM reactions first proposed by Agrawal (*8*) in the oxide environment. Catalytic reaction of vanadyl tetraphenylporphyrin on a sulfided CoMo catalyst led to the generation of several hydrogenated species prior to metal removal. The presence of a sulfur compound, dibenzothiophene, was found to retard the initial porphyrin hydrogenation step but accelerated the overall devanadization rate. In the studies by both Rankel and Kameyama, little emphasis was placed on a quantitative examination of the reaction sequence.

The objective of this paper is to examine more closely the reaction during demetallation of a model nickel compound, namely Ni-tetra(3-methylphenyl)porphyrin, under sulfided catalyst conditions and in the presence of a basic nitrogen compound.

2. EXPERIMENTAL

Experiments were conducted with a model residuum oil comprised of Ni-tetra (3-methylphenyl)porphyrin (Ni-T3MPP) (Midcentury Chemicals, Posen, Ill.) dissolved in a white mineral oil (Nujol). The oil was essentially inert under reaction conditions and was free of sulfur and nitrogen compounds.

Pyridine (Aldrich Chemical Co.) was added as a coreactant to the oil to a level of 100 ppm N to examine the effects of basic nitrogen on the porphyrin reaction.

A commercial $CoO–MoO_3/\gamma\text{-}Al_2O_3$ hydrodesulfurization catalyst (American Cyanamid HDS-16A) was used in this study. The transition metal loadings were 5.7 wt% CoO and 12.2 wt% MoO_3. The catalyst had a unimodal pore size distribution with an average pore diameter of 80.4 Å. Kinetic results were obtained on 170–200 mesh (74 to 88 μm) catalyst particles which had been shown to be free of diffusional limitations. Runs were also conducted under diffusion-limited conditions with $\frac{1}{16}$-in. extrudates. This permitted measurement of intrapellet nickel-deposition profiles.

The catalyst was presulfided using a standard low-temperature procedure recommended by American Cyanamid. The catalyst was heated to 175°C under a flow of helium, followed by a mixture of 10 mole% H_2S in H_2 (Matheson Gas Products) for 6 hr at 175°C and GHSV = 700 hr^{-1}. The temperature was then raised to 315°C at 60°C/hr under this H_2S/H_2 flow and maintained at 315°C for 1 hr. The catalyst was adjusted to demetallation reaction temperature under a purge of helium. During runs on the sulfided catalyst, 0.05 wt% CS_2 (Mallinckrodt) was intentionally added to the feed to stabilize the catalyst in the sulfided state (*10*).

A high-pressure and high-temperature packed-bed flow microreactor (i.d. = 0.52 cm) was used in obtaining intrinsic data.

Calculations and experiments demonstrated the absence of all transport limitations in the system. Runs conducted under diffusion-limited conditions with the $\frac{1}{16}$-in. catalyst extrudates to measure metal-deposition profiles were performed in a larger-diameter (i.d. = 1.75 cm) flow reactor. Both reactors operated in an upflow mode without gas phase. All hydrogen required for reaction was supplied by the porphyrin-containing oil which was first saturated at room temperature with hydrogen at reaction pressure in an autoclave. A system back-pressure of 3.5 MPa (500 psig) higher than the reactor hydrogen pressure combined with the increase in H_2 solubility with temperature ensured that no gas phase formed in the reactor.

Operating conditions ranged from 285 to 345°C and pressures of 4.24 to 10.44 MPa H_2 (600–1500 psig) and contact times, W/Q, of 0.007 to 0.7 g cat. hr/ml oil (LHSV = 1.35–135 hr^{-1}). A full description of the reactor and its operating procedure has been given elsewhere (*8*).

Products formed in the demetallation reactions were determined from analysis of effluent liquid samples. Atomic absorption spectrophotometry was used to determine the total nickel concentration. Ultraviolet–visible spectrophotometry was used at wavelengths of characteristic absorbance to measure the concentrations of the individual porphyrinic species. These procedures are more fully discussed in the thesis of Ware (*9*).

Radial nickel profiles in the $\frac{1}{16}$-in. catalyst extrudates were obtained using an electron microprobe (Applied Research Laboratories Model EMX/SM). The catalyst pellets from specific reactor axial positions were prepared for analysis by washing with xylene in a Soxhlet extractor prior to being mounted in an epoxy resin. The mounted samples were then ground down so that the cross sections at midlength were exposed. A smooth surface for analysis was obtained by a final polishing with 3-μm diamond abrasive paper.

3. KINETIC RESULTS WITH PYRIDINE

Pyridine and quinoline are typical of the heterocyclic nitrogen compounds found in petroleum feedstocks. The lone pair of electrons associated with the nitrogen atom contributes to the basicity of the molecules enabling them to adsorb on $CoMo/Al_2O_3$ sites with both Brønsted and Lewis acid character (*11*). When present with other heteroatom species, they competitively adsorb on active sites and inhibit both HDS and HDN reactions (*10*).

The intrinsic kinetics of Ni-T3MPP demetallation on oxide $CoMo/Al_2O_3$ in the presence of pyridine at 100 ppm N have been investigated. No sulfur compounds were present in the oil. The concentration versus contact time profile for reaction at 345°C and 6.99 MPa H_2 (1000 psig) is presented in Fig. 1. Experimental points are represented

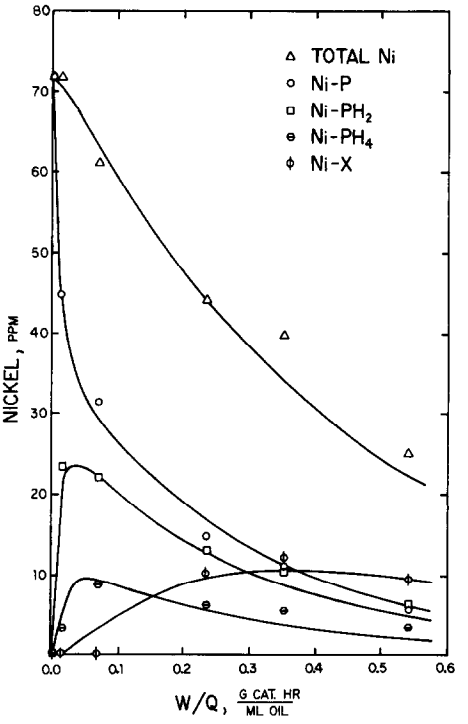

FIG. 1. Concentration versus contact time results for Ni-T3MPP at 71 ppm Ni feed, 345°C, and 6.99 MPa H_2 (1000 psig) with 100 ppm N as pyridine in the feed on the oxide catalyst. Solid lines represent model calculations.

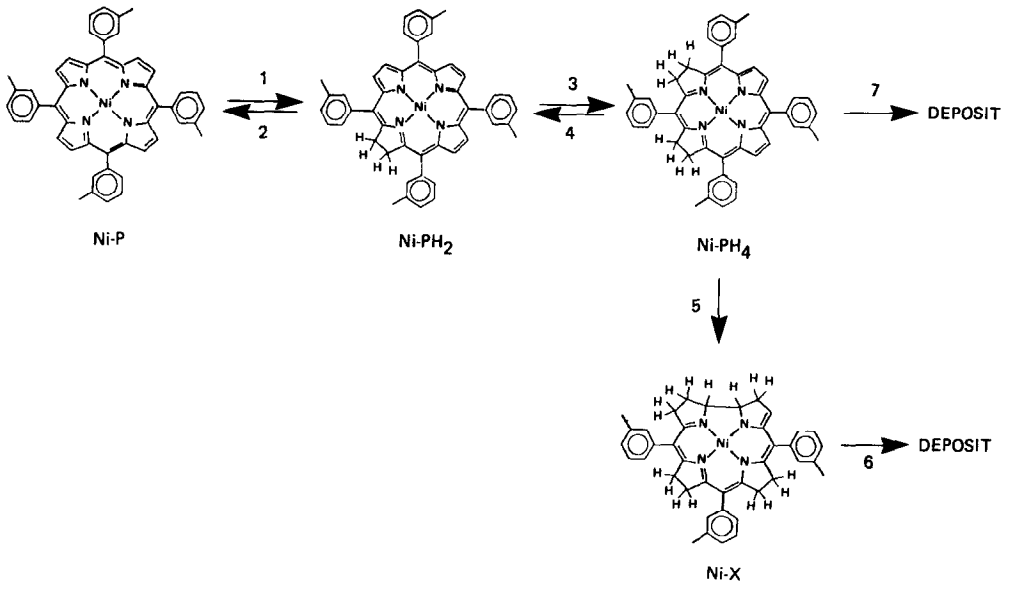

FIG. 2. Reaction sequence for Ni-tetra(3-methylphenyl)porphyrin demetallation.

by the different symbols. Feed porphyrin was rapidly removed in comparison to the total metal, producing the hydrogenated nickel chlorin (Ni-PH_2) and nickel isobacteriochlorin (Ni-PH_4) species. At short contact times (W/Q < 0.06 g cat. hr/ml) the metal balance closed with these species, but at higher conversions the nonporphyrinic Ni-*X* intermediate was present. The nonporphyrinic intermediate constituted no more than 40% of the total metal in the oil at any time. The results reported in Part I (*2*) on the oxide catalyst in the absence of pyridine show that as much as 80% of the metal in the oil was present as this nonporphyrinic species at high feed conversions.

Analysis of effluent oil samples by uv–visible spectroscopy and liquid chromatography revealed no additional nickel-bearing species. This suggests that the demetallation mechanism reported in Part I (*2*) on the oxide catalyst and shown in Fig. 2 has not been changed by the presence of this basic nitrogen compound.

Kinetic rate parameters were determined from the experimental data in Fig. 1 using the sequential hydrogenation/hydrogenolysis model for Ni-T3MPP demetallation developed in Part I, assuming first-order kinetics for each of the reaction steps and constant hydrogen concentration. Presented in Table 1 are the parameters used in the calculated solid curves in Fig. 1, expressed by dividing the rate coefficient by the corresponding rate coefficient on the

TABLE 1

Nitrogen and Sulfur Influence on Ni-T3MPP Reactivity Compared to Clean Oxide Catalyst

$$\text{Ni-P} \underset{k_2}{\overset{k_1}{\rightleftharpoons}} \text{Ni-PH}_2 \underset{k_4}{\overset{k_3}{\rightleftharpoons}} \text{Ni-PH}_4 \xrightarrow{k_7} \text{deposit}$$
$$\text{Ni-PH}_4 \xrightarrow{k_5} \text{Ni-}X \xrightarrow[k_6]{} \text{deposit}$$

Reaction conditions: 345°C, 6.99 MPa H_2 (1000 psig), 65 ppm Ni feed

Reaction step	$k_{pyridine}/k_{oxide}$[a]	$k_{reduced}/k_{oxide}$[b]	$k_{sulfided}/k_{oxide}$[c]
1	0.42	2.5	1.7
2	0.56	2.1	1.7
3	0.35	1.9	2.0
4	0.52	1.4	2.6
5	0.15	2.5	3.5
6	0.61	2.2	7.1
7	0.78	2.2	6.7

[a] Feed contains 100 ppm N as pyridine.
[b] Prereduced catalyst.
[c] Presulfided catalyst.

oxide catalyst in the absence of pyridine. An inhibition is observed for all reaction steps in the presence of this nitrogen compound as all these ratios are less than one.

Satterfield *et al.* (*12*) have reported a decrease in both C–S hydrogenolysis and double-bond hydrogenation rates for thiophene HDS in the presence of pyridine. Similarly, Bhinde (*10*) reported a decrease in all steps in the hydrodesulfurization of dibenzothiophene in the presence of quinoline. Both investigators reported stronger inhibition of the hydrogenation sites compared to the C–S bond scission sites, suggesting that two types of sites poisoned to different extents are present on sulfided $CoMo/Al_2O_3$ and sulfided $NiMo/Al_2O_3$. More recent work by Yang and Satterfield (*13*) has indicated a preferential inhibition by N compounds of hydrogenation sites over the Brønsted acid-like bond-cleavage sites of a sulfided NiMo catalyst.

The degree of inhibition observed for Ni-T3MPP demetallation depends in a similar fashion on the nature of the reaction type, suggesting that multiple sites exist on the oxide form of $CoMo/Al_2O_3$. The hydrogenation/dehydrogenation steps (k_1 to k_4) were all reduced approximately 50% at 100 ppm N, whereas the metal-deposition steps ($k_6 + k_7$) were inhibited to a lesser extent.

Ratnasamy and Knozinger (*11*) report that the majority of pyridine adsorbed on the oxide form of CoMo catalysts is associated with Lewis acid sites such as molybdenum and cobalt vacancies, which are thought to be sites for hydrogenation. Brønsted sites (speculated to possess hydrogenolysis activity) associated with hydroxyl groups on the alumina and Mo showed less affinity for pyridine. Hence the greater reduction observed in hydrogenation activity compared to metal-deposition activity is consistent with the preferred adsorption of pyridine on the metal vacancies or hydrogenation sites.

The observed small contribution of Ni-*X* to the total pool of nickel previously discussed reflects a decline in the reaction selectivity of Ni-PH_4 to Ni-*X* (k_5/k_7). The relative decrease in the rate coefficient for Ni-*X* production compared to direct deposition is the reason for this selectivity drop. The mechanism for Ni-*X* formation, proposed in Part I (*2*), requires both hydrogenation and ring contraction by an acid-catalyzed reaction. Pyridine has been demonstrated to deactivate both of these catalytic functions, giving rise to strong inhibition in Ni-*X* formation.

4. KINETIC RESULTS AND DISCUSSION ON THE SULFIDED CATALYST

Kinetic results on the sulfided catalyst have been obtained for Ni-tetra(3-methylphenyl)porphyrin at 60 ppm Ni over a range of temperatures (285–345°C) and pressures (4.24–10.44 MPa H_2) similar to that reported for the oxide catalyst. Analysis of effluent oil samples has again revealed the presence of only those intermediates that were produced with the oxide catalyst. This is evident in the concentration versus contact time plot presented in Fig. 3 for the reaction at 345°C. Similar arguments used to describe the concentration behavior of nickel species on the oxide catalyst are reiterated here: rapid-feed porphyrin removal occurring concurrently with the production of hydrogenated intermediates; establishment of a dynamic equilibrium between the feed and hydrogenated porphyrins; and initially (after a slightly induction period) a rapid rate of total metal removal followed by, at larger contact times, a slower rate of total metal removal from the nonporphyrinic nickel intermediate. The similarity in reaction mechanism on the sulfided and oxide $CoMo/Al_2O_3$ catalyst is apparent.

Further examination of the sulfided catalyst data at 345°C reveals an enhancement in reaction rates over that reported on the oxide catalyst in Part I. Approximately 80% total nickel removal is achieved at W/Q = 0.075 g cat. hr/ml oil on the sulfided catalyst whereas the equivalent conversion on the

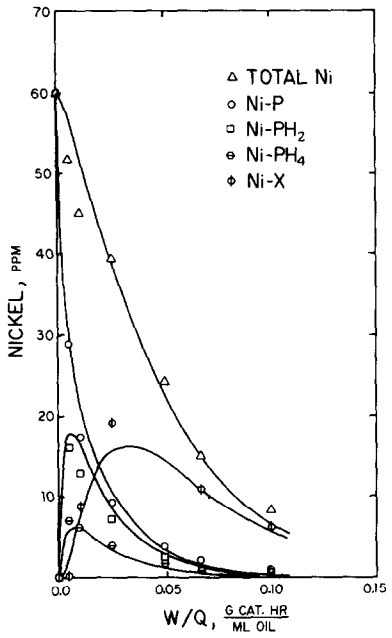

FIG. 3. Concentration versus contact time results for Ni-T3MPP at 60 ppm Ni feed, 345°C, and 6.99 MPa H_2 (1000 psig) on the sulfided catalyst. Solid lines represent model calculations using parameter values in Table 2.

oxide catalyst required a contact time of 0.42 g cat. hr/ml oil.

Increases in hydrodesulfurization reactions are common on sulfided catalysts and are attributed to molybdenum sulfides being the more active catalytic species. Gissy *et al.* (*14*) and Daly (*15*) reported substantially greater benzothiophene conversion on the presulfided catalyst compared to the fresh oxide $CoMo/Al_2O_3$ catalyst. Similarly the presence of H_2S was previously mentioned (*4*) to increase the demetallation of vanadyl tetraphenylporphyrin on an aged $CoMo/Al_2O_3$ catalyst.

Kinetic modeling of the experimental concentration profiles was undertaken using the sequential reaction scheme reported in Part I and shown in Fig. 2. Parameters used in the model solid curves of Fig. 3 are presented in Table 2 with the corresponding activation energies obtained from the Arrhenius plots of Fig. 4. Comparison of the relative magnitude of the individual rate parameters reveals that the metal-deposition steps (k_6, k_7) are rate limiting in the overall demetallation scheme. Metal deposition was likewise rate limiting on the oxide catalyst.

TABLE 2

Ni-Tetra(3-methylphenyl)porphyrin Kinetic Parameters on the Sulfided Catalyst

$$\text{Ni-P} \underset{2}{\overset{1}{\rightleftharpoons}} \text{Ni-PH}_2 \underset{4}{\overset{3}{\rightleftharpoons}} \text{Ni-PH}_4 \xrightarrow{7} \text{deposit}$$
$$\text{Ni-PH}_4 \xrightarrow[6]{5} \text{Ni-}X \rightarrow \text{deposit}$$

Reaction conditions: 345°C, 6.99 MPa H_2 (1000 psig), 60 ppm Ni

Reaction step	k (ml oil/g cat. hr)	E (kcal/mole)	H_2 pressure dependence
1	183.0	23.0	1
2	164.0	24.9	0
3	250.0	19.7	1
4	400.0	23.1	0
5	171.0	40.3	2
6	27.0	29.4	2
7	120.0	20.0	3

At all temperatures the selectivity of $Ni-PH_4$ to Ni-X relative to direct metal deposition (k_5/k_7) was smaller on the sulfided cata-

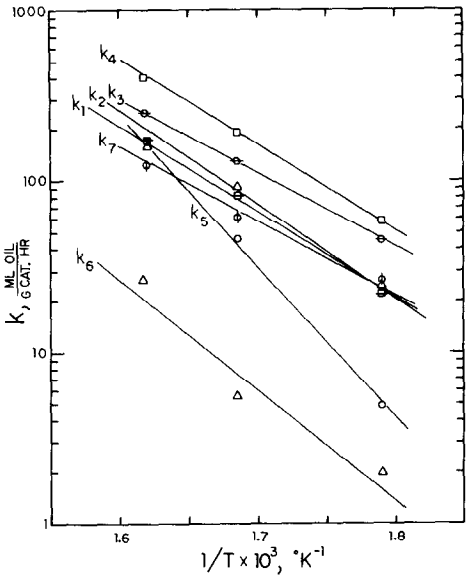

FIG. 4. Arrhenius plots for the first-order rate parameters for Ni-T3MPP at 60 ppm Ni feed and 6.99 MPa H_2 (1000 psig). Sulfided catalyst.

lyst compared to the oxide catalyst. This was a manifestation of the enhanced bond-cleavage activity on the sulfided catalyst promoting ring rupture of the hydrogenated species at the expense of further skeletal rearrangement.

Activation energies for the hydrogenation/dehydrogenation steps (k_1 to k_4) and metal-deposition steps (k_6, k_7) are similar on both the oxide and sulfided catalysts. A substantially larger value, twice that on the oxide catalyst, was obtained for the activation energy of the step producing Ni-X (k_5). A consequence of this large activation energy is that the relative rate of reaction of Ni-PH_4 by direct deposition (k_7) compared to production of Ni-X (k_5) is strongly temperature dependent on the sulfided catalyst. The activation energy difference $E_7 - E_5 = -20.3$ kcal/mole favors direct deposition from Ni-PH_4 at low temperatures on the sulfided catalyst. Only a minor variation in relative rates ($E_7 - E_5 = 4.3$ kcal/mole) was observed with the oxide system toward Ni-X production rather than direct deposition, the former becoming more favored at low temperatures.

The hydrogen-pressure dependence of the kinetic rate parameters was determined over the pressure range 4.24 to 10.44 MPa H_2 (600–1500 psig) at 345°C from the plots in Fig. 5 (the behavior at 285 and 320°C was identical to that at 345°C). The results summarized in Table 2 were similar to those reported for Ni-T3MPP on the oxide catalyst. In this pressure regime on the sulfided catalyst, the hydrogenation steps k_1 and k_3 were first order in hydrogen pressure, consistent with the stoichiometry of the reactions, whereas the dehydrogenation steps k_2 and k_4 showed no hydrogen-pressure dependence. Reaction steps k_5 and k_6 in Fig. 5 exhibited second-order hydrogen dependence, the same behavior observed on the oxide catalyst. The direct metal-deposition step from Ni-PH_4 (k_7) was observed to exhibit an unusually high, third-order dependence on hydrogen. The analogous step on the oxide catalyst was second order in hydrogen. It is difficult to rationalize the third-order dependence even for a step such as this which represents a complex series of reactions. The discrepancy with the oxide catalyst results may reflect a subtle change in the Ni-PH_4 reaction pathway during the apparent direct metal-deposition step on the sulfided catalyst, but the nature of this difference is unclear.

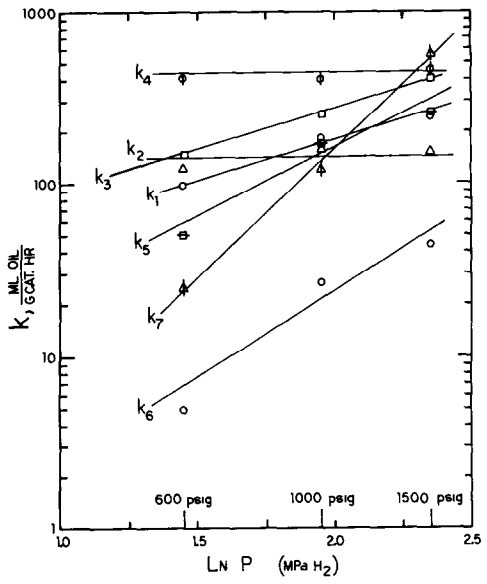

FIG. 5. Hydrogen-pressure dependence for the first-order rate parameters for Ni-T3MPP at 60 ppm Ni feed and 345°C. Sulfided catalyst.

The selective enhancement observed in metal-deposition reactions upon sulfiding the oxide catalyst is quantified in Table 1 where relative rates for each step at 345°C are presented. Also included are data obtained on a prereduced catalyst prepared by *in situ* treatment with hydrogen at 450°C for 4 hr and the nitrogen-poisoning results discussed earlier. Prereduction is shown to increase by approximately twofold the rates of all steps irrespective of the nature of the reaction. A similar doubling in the hydogenation/dehydrogenation rates is observed on the sulfided catalyst, suggesting this may likewise be due to the simultaneous reduction of the catalyst which occurs upon sulfiding (*16*). Such treatment results in creation of anion vacancies on the reduced

molybdenum atoms which have been reported to possess hydrogenation activity (*17*).

The more pronounced impact of sulfiding the catalyst, which is not seen by prereduction, is the dramatic increase in activity for bond-cleavage reactions when compared to the oxide system. The metal-deposition steps (k_6, k_7) are shown to increase by sevenfold in the sulfided environment. This selective enhancement in hydrogenolysis rates is similar to the effect seen with H_2S in the hydrodenitrogenation of quinoline reported by Satterfield and Gultekin (*18*).

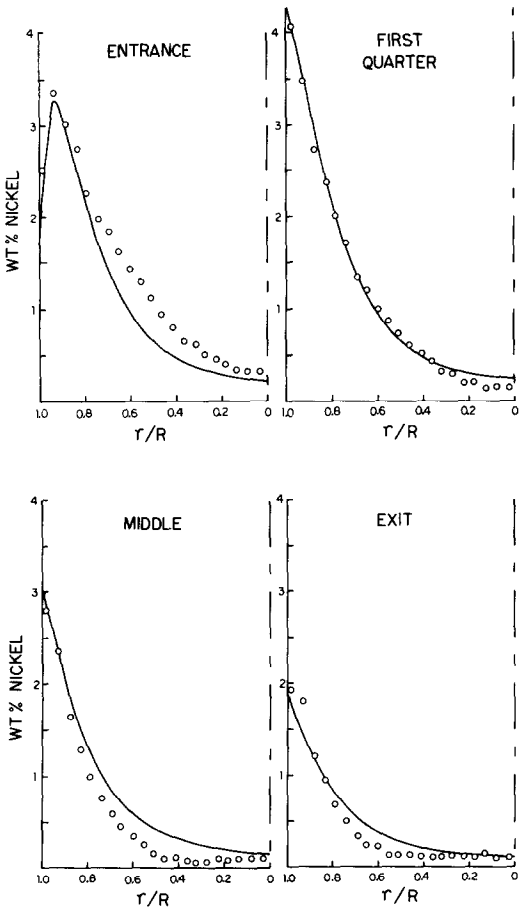

FIG. 6. Nickel-deposition profiles in $\frac{1}{16}$-in.-diameter catalyst pellets at various reactor axial positions from Ni-T3MPP demetallation at 345°C and 6.99 MPa H_2 (1000 psig) on the sulfided catalyst. Solid lines represent model calculations using parameter values in Table 3.

The importance of acid sites reported for hydrogenolysis reactions (*19, 20*) suggests that changes in surface acidity are a contributing factor to the observed reactivity differences in metal-deposition activity on the oxide and sulfided catalysts. Topsøe (*21*) and Sivasanker *et al.* (*22*) have reported the disappearance of strong Brønsted sites associated with surface hydroxyl groups resulting from sulfiding $CoMo/Al_2O_3$ and new Brønsted sites associated with the generation of sulfhydryl groups have been reported by Maternova (*19, 23*). Similarly, Lewis acid sites present as anion vacancies on both catalysts are more prevalent on the sulfided form in the absence of H_2S (*22*).

The enhanced metal-deposition activity observed with the sulfided catalyst is consistent with the concept of new Brønsted sites arising from the dissociation of H_2S recently proposed by Yang and Satterfield (*13*). These investigators have suggested that Lewis sites in the form of molybdenum surface anion vacancies (sites for hydrogenation and hydrogenolysis) on the sulfided catalyst are transformed into Brønsted acid sites (responsible for hydrogenolysis and isomerization) by the dissociation of H_2S into protons and sulfhydryl groups. The presence of H_2S provides a source for continually generating new sites which promote hydrogenolysis reactions through a carbonium ion mechanism. No such transformation of sites occurs in the oxide system under reaction conditions.

5. METAL-DEPOSITION PROFILES ON SULFIDED CATALYST AND DISCUSSION

Metal-deposition profiles obtained under diffusion-limited conditions on the sulfided catalyst are presented in this section. The similarities in the reaction mechanism of Ni-T3MPP observed on the oxide and sulfided catalysts are reflected in the metal profiles. Likewise, the selective enhancement in the rate of metal deposition on the sulfided catalyst is apparent in the metal profiles.

Shown in Fig. 6 are radial nickel-deposition profiles in catalyst pellets as a function of reactor axial position obtained with Ni-T3MPP at 345°C and 6.99 MPa H_2 (1000 psig). The experimental data are represented by the open circles. The internal maximum in metal concentration at the entrance of the bed (M-shape profile) resulting from the sequential reaction scheme shifts rapidly to the edge of the pellet (U-shape profile) a short distance into the reactor as the concentration of metal-depositing species in the bulk increases. Throughout the remainder of the reactor the conventional U-shape profile remains, but the concentrations become increasingly smaller as metal is depleted from the oil.

The profiles once again are dominated by a strong diffusion-limited component resulting in the steep metal gradient at the edge of the pellets, and a relatively diffusion-free component resulting in the more uniform metal concentrations at the center of the pellets. Both characteristics are present throughout the reactor and provide further evidence for the parallel deposition routes in the demetallation scheme for Ni-T3MPP. The selective enhancement in the metal-deposition steps observed upon sulfiding the catalyst is apparent in the sharper profiles and in the proximity of the internal maximum to the edge of the pellet (r/R = 0.93) compared with the oxide results (r/R = 0.75 in Fig. 18 of Part I (*2*)) under identical conditions.

Metal profiles have similarly been obtained with Ni-T3MPP at 345°C and a higher hydrogen pressure of 10.44 MPa H_2 (1500 psig). These results are presented as the open circles in Fig. 7. The higher order hydrogen dependence of the metal-deposition steps discussed in the preceding section on intrinsic reactivity results in a selective enhancement of these reactions as the pressure is raised. This is clearly reflected in the very steep metal profiles throughout the bed and in the inability to experimentally resolve the internal maximum in catalyst pellets at the entrance of the reactor.

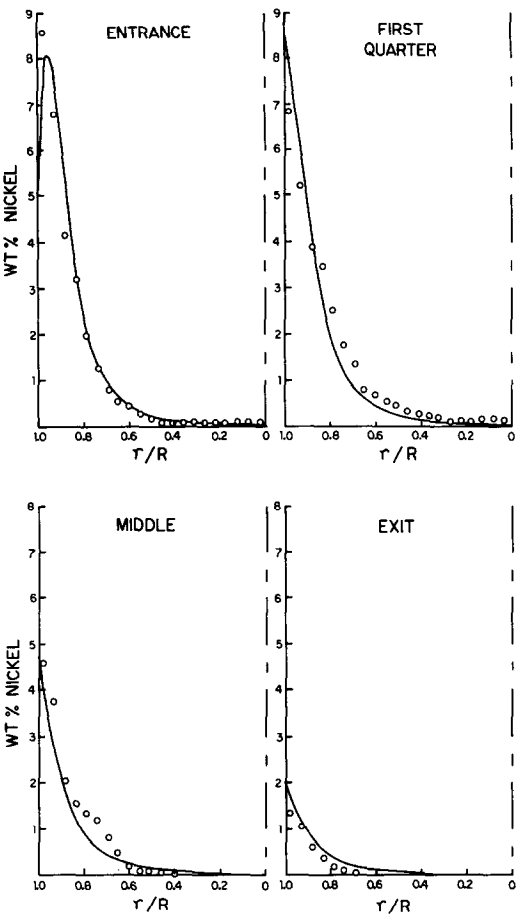

FIG. 7. Nickel-deposition profiles in $\frac{1}{16}$-in.-diameter catalyst pellets at various reactor axial positions from Ni-T3MPP demetallation at 345°C and 10.4 MPa H_2 (1500 psig) on the sulfided catalyst. Solid lines represent model calculations using parameter values in Table 4.

Activity of the catalyst under these conditions is sufficient to achieve over 90% metal removal by the end of the reactor, resulting in the much lower metal loadings observed in pellets taken from the exit.

All metal profiles have been modeled using the coupled diffusion and kinetic reaction scheme developed in Part I (*2*). The parameters in this steady-state model are the seven kinetic rate parameters and the four species diffusion coefficients. These parameters are all assumed to remain constant on the basis that the low level of metal deposited is not sufficient to poison a sub-

stantial number of catalytic sites or constrict diffusion within the pores of the pellets. After the independent determination of the kinetic parameters in the intrinsic reaction studies, the four diffusion coefficients are left as the only unknowns. Estimates for these parameters have previously been obtained in the metal profile modeling on the oxide catalyst. For consistency of the model, these should be applicable on the sulfided catalyst as well.

First attempts to model the metal profiles obtained at 345°C and 6.99 MPa H_2 (1000 psig) were with the corresponding intrinsic kinetic parameters and the oxide catalyst diffusion coefficient values under identical conditions. This set of parameters resulted in a calculated concentration of Ni-*X* 2.5 times higher than experimentally measured in the effluent and a poor agreement between the measured and calculated total metal effluent. Likewise, the model consistently predicted a lower metal loading at the center of pellets than had been measured.

These discrepancies were both corrected by adjustment of the diffusivity of Ni-*X*. A value of 3.5×10^{-6} cm^2/sec resulted in a more satisfactory agreement between experiment and theory than the value of 2.0×10^{-6} cm^2/sec used on the oxide catalyst. The remaining three diffusivities for Ni-P, Ni-PH_2, and Ni-PH_4 were unchanged. The complete set of parameters used in generating the model solid curves in Fig. 6 are listed in Table 3. The features of the experimentally determined profiles are both qualitatively and quantitatively reproduced with the model serving as evidence in support of the reaction scheme developed for Ni-T3MPP and of the accuracy of the kinetic parameters.

The calculated metal profiles of Fig. 7 at the higher hydrogen pressure were determined by a similar procedure using the parameter set in Table 4. In this instance the model was used in a truly predictive fashion. No adjustment of parameters was required to obtain the excellent agreement between the experimental and theoretical profiles throughout the reactor as well as the match in effluent oil composition. The intrinsic kinetic parameters determined on crushed catalyst at the higher hydrogen pressure (10.44 MPa H_2) were used in con-

TABLE 3

Parameters for Ni-Tetra(3-methylphenyl)porphyrin Metal Profile Modeling (Fig. 6)

345°C, 6.99 MPa H_2 (1000 psig), sulfided catalyst

k_1 = 183.0 ml oil/g cat. hr	$D_1 = 1 \times 10^{-6}$ cm^2/sec	t = 84 hr
k_2 = 164.0	$D_2 = 2 \times 10^{-6}$	ρ = 0.88 g/ml
k_3 = 250.0	$D_3 = 2 \times 10^{-6}$	ρ_c = 1.49 g/ml
k_4 = 400.0	$D_4 = 3.5 \times 10^{-6}$	Q = 20 ml/hr
k_5 = 171.0		W = 5.0 g
k_6 = 27.0		R = 0.076 cm
k_7 = 120.0		C_0 = 60 ppm Ni

Effluent oil concentration

	Experimental	Calculated
Ni-P	5.6 ppm Ni	3.6
Ni-PH_2	2.2	2.3
Ni-PH_4	1.0	0.9
Ni-*X*	2.8	4.7
	11.6	11.5

TABLE 4

Parameters for Ni-Tetra(3-methylphenyl)porphyrin Metal Profile Modeling (Fig. 7)

345°C, 10.4 MPa H_2 (1500 psig), sulfided catalyst

k_1 = 240.0 ml oil/g cat. hr	$D_1 = 1 \times 10^{-6}$ cm²/sec	t = 69.5 hr
k_2 = 150.0	$D_2 = 2 \times 10^{-6}$	ρ = 0.88 g/ml
k_3 = 400.0	$D_3 = 2 \times 10^{-6}$	ρ_c = 1.49 g/ml
k_4 = 450.0	$D_4 = 3.5 \times 10^{-6}$	Q = 25 ml/hr
k_5 = 246.0		W = 5.0 g
k_6 = 44.0		R = 0.076 cm
k_7 = 560.0		C_0 = 61 ppm Ni

Effluent oil concentration

	Experimental	Calculated
Ni-P	2.3 ppm Ni	2.3
Ni-PH_2	1.0	1.3
Ni-PH_4	0.5	0.4
Ni-X	1.2	2.2
	5.0	6.2

junction with the values for the four diffusion coefficients used at 6.99 MPa H_2 on the sulfided catalyst.

The consistency of the diffusion coefficients for the four nickel species present in the oil with changes in the nature of the catalyst and operating conditions is encouraging in terms of verifying the reliability of the model. Liquid-phase diffusivities are relatively insensitive to pressure changes of this magnitude. Similarly, a variation of these parameters with a change from the oxide to the sulfided catalyst would be expected only if solid support interactions such as adsorption or surface diffusion contributed in a substantially different manner to the apparent diffusion coefficients. The difference in value for the diffusion coefficient of Ni-*X* on the oxide and sulfided catalysts, while not large, was necessary to achieve the better fit. Similarly, using this larger value to interpret the metal profiles on the oxide catalyst in Part I (*2*) resulted in poorer agreement. No explanation was evident as to why this one diffusion coefficient should vary between the two catalysts. A larger value for the structurally smaller Ni-*X* molecule is consistent from a hydrodynamic standpoint, but the magnitude of the change is not large and cannot be realistically interpreted for a lumped parameter such as this.

6. CONCLUSIONS

The presence of pyridine on an oxide catalyst in the absence of sulfur, or reaction without pyridine on a sulfided catalyst, did not change the demetallation pathway for Ni-T3MPP on a $CoMo/Al_2O_3$ catalyst. Reaction occurs through the same stable intermediates observed on the clean (N and S free) oxide form of the catalyst with multiple hydrogenation steps preceding the generally slower, rate-limiting, metal-deposition steps in the overall sequence. The reactivity of Ni-T3MPP on the sulfided catalyst has temperature and hydrogen-pressure dependencies for the individual steps in the demetallation sequence which are similar to those previously discussed for the oxide system. The consistency of the proposed demetallation pathway has been further demonstrated by the success achieved in modeling the pattern of metal deposition in catalyst pellets throughout the reactor in both the oxide and sulfided sys-

tems using diffusion coefficients on the order of 10^{-6} cm^2/sec. Agreement such as this justifies the extrapolation of information obtained on demetallation pathways with the clean (N and S free) oxide system to more complex environments.

While no mechanistic differences have been observed in the presence of basic nitrogen or on a sulfided surface, a potentially important difference in reaction selectivity has been noted. The relative hydrogenation to hydrogenolysis rate constants within the demetallation sequence in the presence of nitrogen and sulfur were found to vary substantially compared to the clean oxide system. Basic nitrogen in the form of pyridine was observed to strongly deactivate the hydrogenation sites (k_1 to k_4) but showed less inhibition on the metal-deposition (hydrogenolysis) steps (k_6 and k_7). Similarly, sulfiding the $CoMo/Al_2O_3$ catalyst was shown to enhance the metal-deposition steps (k_6 and k_7) by a factor of 7 compared to only a twofold increase in the hydrogenation/dehydrogenation reactions (k_1 to k_4).

This leads to the conclusion that at least two separate types of sites are responsible for the overall demetallation reaction. The hydrogenation sites are sensitive to nitrogen poisoning and only moderately activated by sulfiding (most likely through reduction). The hydrogenolysis or metal-deposition sites are less sensitive to nitrogen poisoning and are strongly activated by sulfiding, possibly via generation of increased Brønsted acidity. This suggests the possibility of using nitrogen compounds to improve the selectivity of a catalyst for metal removal relative to hydrogenation. Bhinde (*10*) and Satterfield *et al.* (*12*) have previously discussed a similar situation where pyridine was used to improve the selectivity of a catalyst for hydrodesulfurization (i.e., hydrogenolysis) relative to hydrogenation.

The presence of N and S was also shown to decrease the reaction selectivity of Ni-PH_4 to Ni-X (k_5/k_7). The relatively slow demetallation of this nonporphyrinic species (k_6) is desirable from the standpoint of obtaining uniform metal deposits in catalyst pellets.

An important consequence of this ability to alter the relative hydrogenation/hydrogenolysis rates within the demetallation sequence is the potential improvement in catalyst performance and lifetime through control of metal-deposition location. The influence of this hydrogenation/hydrogenolysis selectivity on the intrapellet metal distribution can be substantial, as has been demonstrated by the differences between the oxide and sulfided catalyst metal profiles.

ACKNOWLEDGMENTS

The authors are grateful to David Green, Chi-Wen Hung, Jack T. Gilmore, and Mark J. Meisner of Chevron Research Company for providing the microprobe measurements in Figs. 6 and 7. The authors are also grateful for the many helpful discussions with David Green and Chi-Wen Hung. The financial support of the National Science Foundation, Grant CPE 80-20852, and Chevron Research Company is also gratefully acknowledged.

REFERENCES

1. Yen, T. F., "The Role of Trace Metals in Petroleum." Ann Arbor Science Pub. Ann Arbor, Mich., 1975.
2. Ware, R. A., and Wei, J., **93,** 100 (1985).
3. Rankel, L. A., *ACS Prepr. Div. Pet. Chem.* **26**(3), 689 (1981).
4. Rankel, L. A., and Rollmann, L. D., *Fuel* **62,** 44 (1983).
5. Hung, C. W., and Wei, J., *Ind. Eng. Chem. Process Des. Dev.* **19,** 250, 257 (1980).
6. Kameyama, H., Sugishima, M., Yamada, M., and Amano, A., *J. Jpn. Pet. Inst.* **24,** 317 (1981).
7. Kameyama, H., and Amano, A., *J. Jpn. Pet. Inst.* **25,** 118 (1982).
8. Agrawal, R., and Wei, J., *Ind. Eng. Chem. Process Des. Dev.* **23,** 505, 515 (1984).
9. Ware, R. A., "Reactivity of Nickel Porphyrins in Catalytic Hydrodemetallation," Sc.D. thesis. M.I.T., September 1983.
10. Bhinde, M. V., "Quinoline Hydrodenitrogenation Kinetics and Reaction Inhibition," Ph.D. thesis. University of Delaware, June 1979.
11. Ratnasamy, P., and Knozinger, H., *J. Catal.* **54,** 155 (1978).
12. Satterfield, C. N., Modell, M., and Wilkens, J. A., *Ind. Eng. Chem. Process Des. Dev.* **19,** 154 (1980).

13. Yang, S. H., and Satterfield, C. N., *J. Catal.* **81,** 168 (1983).
14. Gissy, H., Bartsch, R., and Tanielian, C., *J. Catal.* **65,** 150 (1980).
15. Daly, F. P., *J. Catal.* **51,** 221 (1978).
16. Chin, R. L., and Hercules, D. M., *J. Phys. Chem.* **86,** 3079 (1982).
17. Grange, P., *Catal. Rev. Sci. Eng.* **21,** 135 (1980).
18. Satterfield, C. N., and Gultekin, S., *Ind. Eng. Chem. Process Des. Dev.* **20,** 62 (1981).
19. Maternova, J., *Appl. Catal.* **6,** 61 (1983).
20. Katzer, J. R., Stiles, A. B., and Kwart, H., US-DOE Report DOE/ET/03297-1. Washington, 1980.
21. Topsøe, N., *J. Catal.* **64,** 235 (1980).
22. Sivasanker, S., Ramaswamy, A. V., and Ratnasamy, P., *in* "Proceedings, Climax Third International Conference on the Chemistry and Uses of Molybdenum" (H. F. Barry and P. C. H. Mitchell, Eds.), p. 98. Climax Molybdenum Co., Ann Arbor, Mich., 1980.
23. Maternova, J., *Appl. Catal.* **3,** 3 (1982).